Free-edge stress fields in generic laminated composites via higher-order kinematics

Free-edge stress fields in generic laminated composites via higher-order kinematics

A.G. de Miguel[*1], A. Pagani[†1], and E. Carrera[‡1]

[1]MUL[2] Group, Department of Mechanical and Aerospace Engineering, Politecnico di Torino, Turin, Italy

Abstract

The present work introduces a numerical approach for the study of the free-edge effects that arise in generic laminated composites with arbitrary geometries. The model is based on the use of a higher-order beam theory that employs only displacement unknowns over the cross-section domain, the so-called Lagrange expansion (LE). This allows for the representation of arbitrary sections of laminated structures through a two-dimensional distribution of mathematical domains, accounting for layerwise (LW) kinematics and high refinements towards the free edges. Subsequently, the finite element method (FEM) is employed to solve the problem along the laminate's length, thus enabling the user to introduce arbitrary boundary conditions. Benchmark solutions of the free-edge stresses in symmetric laminates under extension, bending and twisting are included to assess the model. Then, new solutions of a composite C-section beam made of an asymmetric lamination are provided.

Keywords: Free-edge, Laminates, Carrera Unified Formulation, Finite Element Method, Stress concentrations.

[*]Ph.D. Student, alberto.garcia@polito.it
[†]Assistant Professor, alfonso.pagani@polito.it
[‡]Professor of Aerospace Structures and Aeroelasticity, erasmo.carrera@polito.it

1 Introduction

The increasing adoption of composite laminates in the construction of new lightweight structures demands a comprehensive knowledge of their mechanical response at different scales. Unlike traditional thin-walled metallic structures, laminates are inherently heterogeneous and feature abrupt changes of the material properties through the thickness, see the book of Jones [1]. Although this allows for the optimization of the material to a desired performance, it also provokes some unwanted effects such as stress concentrations in holes, joints and free edges, that must be fully understood for the safe deployment of composite parts. In particular, the so-called free-edge effects refer to singular stress states that arise at the interfaces between dissimilar layers in the vicinity of geometrical or mechanical discontinuities in the structure. An illustration of the free-edge effects in typical composite beams is shown in Fig. 1. The present paper introduces a numerical method for the efficient evaluation of the free-edge stresses in generic composite laminated structures.

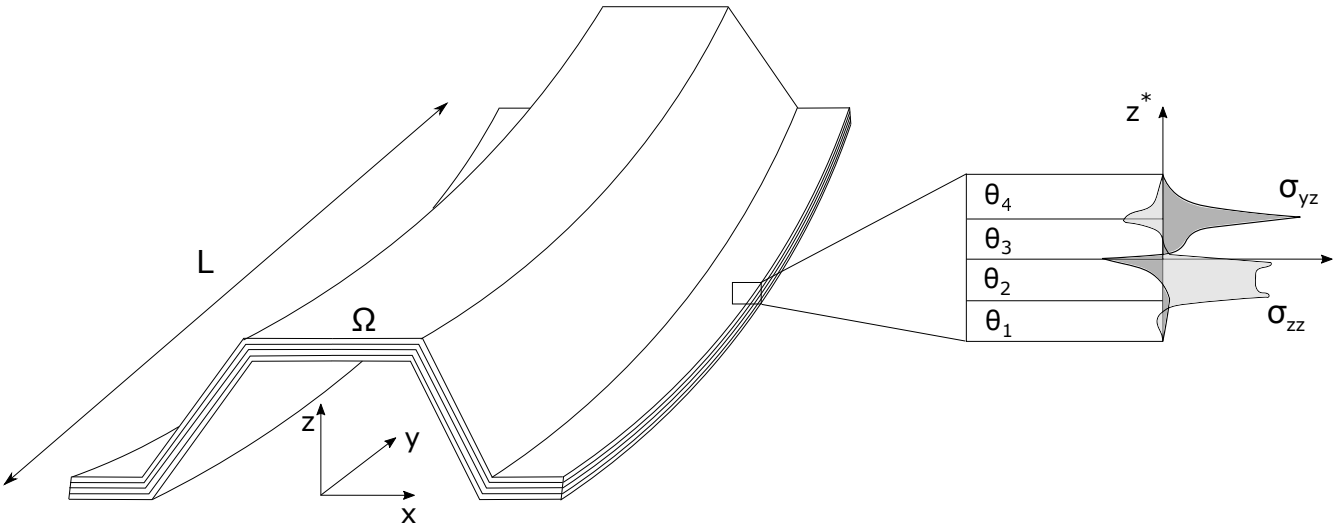

Figure 1: Free-edge stresses in generic composite beams.

Classical laminate theories cannot provide any useful information of the free-edge effects, therefore specific models continue to be developed for understanding the mechanics of this complex problem. The first studies addressing the topic were carried out by Hayashi [2] and Puppo and Evensen [3]. Then, in 1970 Pipes and Pagano [4] provided the first approximation of the 3D stress fields at the free edges. The latter work was followed by numerous studies, which have made the literature rich in analytic and numerical solutions for the free-edge problem, as illustrated in the excellent review of Mittelstedt and Becker [5]. However, given the high complexity and singular nature of the interlaminar stress fields, no exact elasticity solution is available yet for the free-edge stress fields and active interest is still focused nowadays in the development of accurate tools for their evaluation in real composite applications. In most studies, the benchmark example for the free-edge study is that defined in [4], which addresses a symmetric cross-ply laminate of infinite

length loaded under uniaxial extension. In that case, the solutions become independent of the longitudinal direction and the problem is reduced to the section domain. Due to the Poisson effect and the diverse elastic moduli of the material, the plies tend to behave differently in the in-plane direction. Subsequently, in order to satisfy the compatibility of the displacements at the interfaces, transverse shear stresses appear in a small zone near the free edge and, consequently, the fulfillment of the equilibrium conditions lead to a full 3D state of stress which features singularities at the interfaces, see Fig 1. A correct evaluation of these stresses, which can infer damage to the material due to the onset of delamination, becomes then necessary for the design of composite structures. An overview of some of the most relevant solutions of the free-edge problem which are available in the literature is included in the following.

Since the initial investigations addressing the singularities at the free edges, many close-form approaches have been introduced to provide an accurate approximation of the stress fields. As an extension of their early research, Pipes and Pagano [6] proposed an approximate elasticity solution using a Fourier series for the displacements. Then, Pagano [7] employed a modified version of the higher-order theory of Whitney and Sun [8] to provide an analytic solution of the interlaminar normal stresses in symmetric composite laminates. Kassapoglou and Lagace [9] used the force balanced method and the principle of minimim complementary energy to solve the interlaminar stresses in angle-ply and cross-ply laminates. Becker [10] introduced a single-layer higher-order theory with a warping mode in the free-edge area. The stress functions of Lekhnitskii [11] were employed by Yin [12] to develop a stress-based layerwise model for the evaluation of the interlaminar stresses in a laminate strip under combinations of extension, bending and twisting. Tahani and Nosier [13] presented a displacement-based analytical solution of uniformly loaded composite laminates based on the layerwise theory of Reddy [14]. An approximate stress function was introduced by Flanagan [15] using an expansion of harmonic terms in the thickness direction and the princple of minimum complimentary energy. An iterative method to solve the free-edge stresses based on the extended Kantorovich method was employed by Cho and Yoon [16] for uniaxial extension. In a further development, Cho and Kim [17] extended the method to study also bending, twisting and thermal loads. More recently, Dhanesh et al. [18] introduced the mixed-field multiterm Kantorovich method using the Reissner's mixed variational theorem [19] to satisfy all boundary conditions at the free-edges and the interlaminar continuity.

Numerical approaches have also been considerably popular to provide the 3D stress solutions at the free edges. Among these, special mention is due to the pioneering work of Pipes and Pagano [4], who used the finite difference method (FDM) to compute the 3D displacements and stresses in symmetric laminates. In the following years, the finite element method (FEM) has been employed in most of the works on free-edge due to its availability and versatility, commonly to generate 2D plane strain models. Wang and Crossman [20] made an study of the interlaminar singularities in symmetric laminates using three-node elements with a mesh refinement in the free-edge zone.

Whitcomb et al. [21] performed an extensive study on the reliability of the FEM for the study of stress singularities using eight-node elements, reporting that the stress solutions obtained are accurate except for the two elements in the vicinity of the singularity. Although computationally more expensive, 3D solid elements have also been employed to solve the free-edge problem by Raju and Crews [22] and Lessard et al. [23], among others. Recently, Martin et al. [24] compared the accuracy of 2D and 3D finite elements for the onset of delamination due to shear in angle-ply laminates. Solutions of the free-edge stresses were also obtained via the boundary element method by Davì and Milazzo [25] and the boundary finite element method by Lindemann and Becker [26].

Non-traditional FE models based on plate/beam theories of structures have also been used to obtain 3D stress fields at the free-edge. Robbins and Reddy [27] implemented a higher-order layerwise plate element to study 3D-like localized effects in composite laminates, showing interesting advantages in comparison to 3D solid models, such as faster element stiffness integration and simplified input requirements. D'Ottavio et al. [28] proposed a number of displacement-based and mixed plate elements with higher-order kinematics for the study of the interlaminar stresses at the free-edges. Vidal et al. [29] used the proper generalized method to split the problem in the 2D in-plane domain, modeled via eight-node elements, and a 1D analysis on the thickness direction, represented by a layerwise fourth-order expansion. In a recent publication, Peng et al. [30] employed the mechanics of structure genome to study the free-edge effects in composite beams featuring generic laminations via a refined cross-sectional analysis.

This paper introduces a numerical approach based on higher-order 1D models for the free edge analysis of generic composite beams. The Carrera's unified formulation [31] is employed to generate a theory of structure which makes use of displacements as only variables and Lagrangian polynomials as cross-sectional assumptions, named as Lagrange expansion (LE). This theory of structures was first introduced by Carrera and Petrolo [32] and has proven to be a powerful tool for the accurate stress analysis of composite beams in many works, see [33, 34, 35]. The use of a distribution of mathematical expansion domains to assume the deformation of the cross-section of the laminated beam enables the model to capture 3D-like stress distributions at the ply level. Moreover, it also allows the user to refine the cross-section domain in the zones of interest, such as the free-edges. The accuracy and robustness of the proposed method to represent the free-edge effects in generic composite beams is presented in the present work.

The paper is organized as follows: Section 2 introduces the LE beam theory employed in the present study and its application to the analysis of the free-edge effects in laminated beams with arbitrary cross-sections. Subsequently, the FEM solution of the problem is presented in Section 3, including the derivation of the fundamental nucleus of the stiffness matrix and the integrals of the beam element. Then, the numerical assessment of the proposed method is included in Section 4, which includes benchmark examples and a realistic application. Finally, the conclusions are summarized in Section 5.

2 Layerwise laminated theories based on a Lagrange Expansion

Many displacement-based theories of structure have been introduced in the past decades for the study of the mechanical response of laminated structures. These theories are usually divided into two classes: equivalent-single layer (ESL) and layerwise (LW). In the former, the displacement assumptions are taken for the whole thickness of the laminate and the number of variables is therefore independent of the number of layers. On the other hand, LW theories make use of independent assumptions for each layer, leading to a quasi-3D model in which the number of degrees of freedom grows as the number of layers increases. ESL theories are very attractive due to their lower computational costs and they are extensively employed by engineers to acquire information about the global response of the composite structure. However, these theories, which in most cases make use of C^1 kinematics across the stack of plies, are not suitable to provide accurate 3D stress fields at the ply level, specially in thick laminates, or in particularly complex zones, such as open holes or free-edges.

Despite the higher computational demands, LW models [36, 37, 38, 39, 40] provide more information of the meso-scale effects by accounting for the deformation of each ply independently. In this class of theories, the C^0 continuity of the displacements must be imposed at the interfaces between layers by a certain numerical constrain, such as specific displacement functions or Lagrange multipliers. Reddy [14, 41] introduced an elegant solution using 1D elements to discretize the thickness of the laminate which satisfy the continuity conditions automatically. By taking displacement assumptions at the ply-level, LW models are able to capture the zig-zag effect of the displacements in the thickness direction, which is strongly related to the complex distribution of transverse stresses in composite laminates, as noted by Carrera [42].

In the framework of CUF for beam theories, the LW displacement field of the composite beam is written as:

$$\mathbf{u}(x, y, z) = F_\tau(x, z)\mathbf{u}^k_\tau(y) \quad \tau = 1, 2, ..., M \tag{1}$$

where $\mathbf{u}(x, y, z)$ is the three-dimensional displacement field, $\mathbf{u}_\tau(y)$ is the vector of generalized displacements that depends on the longitudinal coordinate y and $F_\tau(x, z)$ are the expansion functions of the cross-sectional domain. The class and number of expansion functions is arbitrary, being M the maximum number of expansions, which is a user defined parameter. Repeating indexes denote summation.

2.1 Lagrange Expansions

Lagrange Expansions (LE) are an extension of the Reddy's LW theory to the beam analysis. This beam theory, introduced by Carrera and Petrolo [32], is based on the use of interpolating Lagrange

polynomials as expansion functions F_τ of the cross-sectional coordinates. In this manner, the cross-section of the composite beam can be discretized with an arbitrary number of Lagrangian domains, which are used to represent the surfaces of each layer. The explicit expressions of a nine-node quadratic expansion (hereinafter denoted to as L9) are reported in the following:

$$\begin{gathered} F_\tau = \tfrac{1}{4}(r^2 + rr_\tau)(s^2 + ss_\tau) \qquad \tau = 1,3,5,7 \\ F_\tau = \tfrac{1}{2}s_\tau^2(s^2 - ss_\tau)(1 - r^2) + \tfrac{1}{2}r_\tau^2(r^2 - rr_\tau)(1 - s^2) \qquad \tau = 2,4,6,8 \\ F_\tau = (1 - r^2)(1 - s^2) \qquad \tau = 9 \end{gathered} \tag{2}$$

where r and s are the coordinates of the natural plane [-1,1]×[-1,1] and r_τ and s_τ are the position of the nodes. Since LE beam models make use of displacement unknowns as degrees of freedom, they represent a useful tool for the efficient stress analysis of beam-like structural components. Moreover, LE are in particular interesting to generate LW models since the displacement compatibility at the interfaces between plies is automatically satisfied with no need of numerical artifacts.

2.2 High-fidelity beam models for free-edge analysis

Free-edge effects are confined in a small zone whose size is directly proportional to the thickness of the laminate, as reported in the experimental work of Pipes [43]. Subsequently, in the damage analysis of laminated structures, a refinement of the model is required towards the free edge, see for instance the works of Wang and Crossman [20], Martin et al. [24] and Saeedi et al.[44]. In LW theories, a common technique for the refinement of the stress solutions is the use of mathematical layers within the thickness of each ply.

LE beam models extend this technique to the whole cross-section domain, allowing the user to generate arbitray distributions of mathematical domains over the laminate's section, refining the free edge zone with denser distributions. Moreover, any cross-section geometry can be represented using a mesh of LE domains. Figure 2 shows the cross-section of a composite C-section beam modeled with multiple mathimatical layers and a refinement towards the bottom and top free edges. It is worthy to mention that one could straightforwardly generate different classes of mathematical domains based on Lagrange polynomials, such as three-node, six-node ot sixteen-node expansions, although this implementation remains out of the scope of the present work. If the reader is interested, the development of such theories of structure is reported in the book by Carrera et al. [31].

3 Finite element approximation

Several methods can be applied to solve the mechanical problem in the longitudinal direction, including strong and weak form solutions. In the present study, the FEM is chosen due to is easy

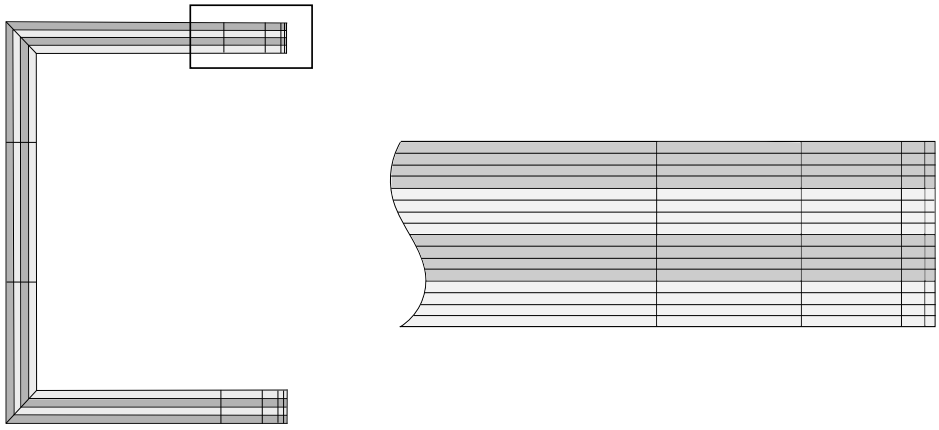

Figure 2: Distribution of LE domains over the cross-section of a C-section laminated beam.

implementation and versatility. In the 1D FE framework, the displacement unknowns, $\mathbf{u}_\tau$, are interpolated over the beam axis using standard shape functions, N_i, as:

$$\mathbf{u}_\tau^k(y) = N_i(y)\mathbf{u}_{\tau i}^k, \qquad i = 1, 2, ..., n, \tag{3}$$

where $\mathbf{u}_{\tau i} = \{u_{x_{\tau i}}\ u_{y_{\tau i}}\ u_{z_{\tau i}}\}^T$ is the vector of the displacement unknowns and n is the total number of nodes. In the present work, four-node cubic Lagrangian elements are employed in all numerical cases. Subsequently, introducing Eq. 3 into the kinematic field of the beam, Eq. 1, the global displacements can be described as:

$$\mathbf{u}(x, y, z) = F_\tau(x, z)N_i(y)\mathbf{u}_{\tau i}^k. \tag{4}$$

The principal of virtual displacements (PVD) for linear static problems is now recalled to obtain the governing equations. The PVD states

$$\delta L_{int} = \int_L \int_\Omega \delta\boldsymbol{\varepsilon}^T \boldsymbol{\sigma}\, d\Omega\, dy = \delta L_{\text{ext}}, \tag{5}$$

i.e. the equivalence of the virtual variation of the strain energy, δL_{int}, and the virtual variation of the work of done by the external loads, δL_{ext}. Subsequently, recalling the geometrical and constitutive relations, the expression of the strain energy reads:

$$\delta L_{int} = \int_L \int_\Omega \delta\mathbf{u}_{\tau i}^{kT}[\boldsymbol{D}^T(F_\tau N_i \boldsymbol{I})\tilde{\mathbf{C}}^k \boldsymbol{D}(F_s N_j \boldsymbol{I})]\mathbf{u}_{sj}^k\, d\Omega\, dy \tag{6}$$

where $\boldsymbol{D}$ is the differential operator and $\tilde{\mathbf{C}}^k$ is the material matrix of the k-th layer in the global coordinate system shown in Fig. 1. The geometrical and constitutive equations are detailed in

Appendix A. Reformulating Eq. (6), one can write

$$\delta L_{\text{int}} = \delta \mathbf{u}_{\tau i}^{T} \mathbf{K}^{\tau s i j} \mathbf{u}_{s j}, \tag{7}$$

where $\mathbf{K}^{\tau s i j}$ is the *fundamental nucleus* of the stiffness matrix. The layer index k has been omitted in Eq. (7) for the sake of clarity. The fundamental nucleus is the 3×3 matrix which contains the essential information of the beam model. The derivation of the corresponding loading vector is not included here, but it can be found in [31]. An example of two components of $\mathbf{K}^{\tau s i j}$ is included in the following:

$$\begin{aligned} K_{xx}^{\tau s i j} &= \widetilde{C}_{22}\, I_{ij}\, E_{\tau_{,x} s_{,x}} + \widetilde{C}_{44}\, I_{ij}\, E_{\tau_{,z} s_{,z}} + \widetilde{C}_{26}\, I_{ij,y}\, E_{\tau_{,x} s} + \widetilde{C}_{26}\, I_{i,y j}\, E_{\tau s_{,x}} + \widetilde{C}_{66}\, I_{i,y j,y}\, E_{\tau s} \\ K_{xy}^{\tau s i j} &= \widetilde{C}_{23}\, I_{ij,y}\, E_{\tau_{,x} s} + \widetilde{C}_{45}\, I_{ij}\, E_{\tau_{,z} s_{,z}} + \widetilde{C}_{26}\, I_{ij}\, E_{\tau_{,x} s_{,x}} + \widetilde{C}_{36}\, I_{i,y j,y}\, E_{\tau s} + \widetilde{C}_{66}\, I_{i,y j}\, E_{\tau s_{,x}}. \end{aligned} \tag{8}$$

The remaining components of the fundamental nucleus can be obtained by permutations from Eq. 8. The I and E terms of the previous expression correspond to the integrals over the length of the beam, L, and over the section surface, Ω, respectively. The comma indicates partial derivation with respect to the global coordinates. For the sake of completeness, the explicit expressions of the E terms are shown:

$$\begin{aligned} E_{\tau_{,x} s_{,x}} &= \int_\Omega F_{\tau,x} F_{s,x}\, d\Omega, \quad E_{\tau_{,z} s_{,z}} = \int_\Omega F_{\tau,z} F_{s,z}\, d\Omega, \quad E_{\tau s} = \int_\Omega F_\tau F_s\, d\Omega, \\ E_{\tau_{,x} s_{,z}} &= \int_\Omega F_{\tau,x} F_{s,z}\, d\Omega, \quad E_{\tau_{,z} s_{,x}} = \int_\Omega F_{\tau,z} F_{s,x}\, d\Omega, \quad E_{\tau_{,x} s} = \int_\Omega F_{\tau,x} F_s\, d\Omega, \\ E_{\tau s_{,x}} &= \int_\Omega F_\tau F_{s,x}\, d\Omega, \quad E_{\tau_{,z} s} = \int_\Omega F_{\tau,z} F_s\, d\Omega, \quad E_{\tau s_{,z}} = \int_\Omega F_\tau F_{s,z}\, d\Omega; \end{aligned} \tag{9}$$

as well as the expression of the I terms:

$$\begin{aligned} I_{ij} &= \int_l N_i\, N_j\, \mathrm{d}y, \quad I_{i,y j} = \int_l N_{i,y}\, N_j\, \mathrm{d}y, \\ I_{ij,y} &= \int_l N_i\, N_{j,y}\, \mathrm{d}y, \quad I_{i,y j,y} = \int_l N_{i,y}\, N_{j,y}\, \mathrm{d}y. \end{aligned} \tag{10}$$

All the integrals are solved numerically using standard quadrature rules.

The fact that the integrals of the energy terms in the fundamental nucleus are decoupled into the cross-section domain and the axial length provides an interesting framework for the study of laminated composites, in which the classical laminate assumptions hold (to an extent) over most the volume and localized 3D effects arise in particular zones. This property can be exploited to drastically reduce the computational size of the free-edge problem in composite beams, in which the mechanical solutions vary smoothly along y, while feature massive gradients over the cross-section

coordinates in the vicinity of the free-edge. Indeed, most of the solutions in the literature (weak and strong) are based in the assumption of plane strains, which accounts for a laminate of infinite length and neglects any variation of the solutions in the longitudinal direction. Models based in this assumption can produce very accurate stress solutions over the section domain, although they are always limited to simple geometries and boundary conditions, being in most cases allocated to benchmarking purposes. By employing the FEM to solve the structural problem, generic composite problems can be straightforwardly addressed, as it is illustrated in Fig. 3.

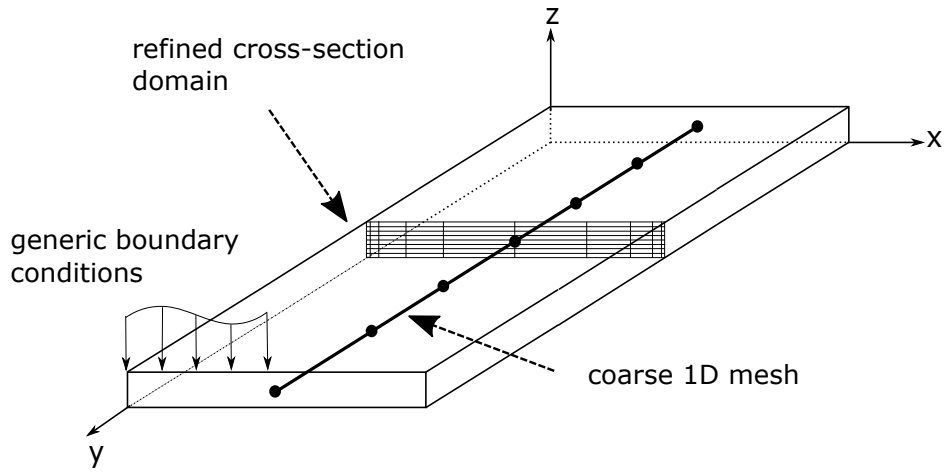

Figure 3: Representation of the FEM modeling of composite laminates using LE beam elements.

4 Numerical results

The numerical assessment of the present method for the free-edge analysis of composite laminates is divided in two main sections. The first part includes a comprehensive assessment of the solutions against well-known benchmark results of the Pipes and Pagano laminate [4] under extension, bending and twisting loads. Secondly, the advanced capabilities for the efficient study of complex composite beams is presented through an example of a laminated C-section beam.

4.1 Assessment through benchmark problems

To assess the present model for the free-edge analysis under generic loads a series of benchmark examples from the literature are selected. The material and geometry are equivalent to that of the pioneering work of Pipes and Pagano [4], who considered a symmetric cross-ply with four layers

of equal thickness, $t = h/4$. The material properties are the following:

$$\begin{aligned} &E_1 = 137.9\ GPa, \quad E_2 = E_3 = 14.5\ GPa, \\ &G_{12} = G_{13} = G_{23} = 5.9\ GPa, \\ &\nu_{12} = \nu_{13} = \nu_{23} = 0.21. \end{aligned} \tag{11}$$

Although most of the studies on free-edge are based on 'Psi' units, the SI is adopted in the present work. The section of the laminate features a width-to-thickness ratio, b/h, is equal to 4, whereas the length is assumed as infinite. In order to generate a model making use of beam elements, it is necessary to specify finite dimensions. Thus, in all the examples included in the present section $b = 20$ mm, $h = 5$ mm and $L = 400$ mm, as shown in Fig. 4. The total length, L, is chosen great enough to neglect the local effects at the zones of application of the boundaries, resulting in a slenderness ratio of $L/b = 20$.

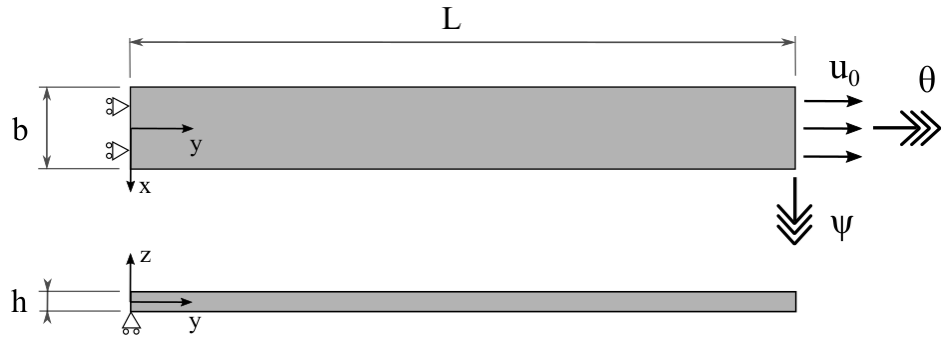

Figure 4: Dimensions of the four-layer laminate used for benchmarking and different loads considered.

Results are obtained for extension, bending and twisting loads. Since the FEM is employed to solve the governing equations of the problem, any boundary condition can be considered. The model generated for the present assessment consists of 6 cubic 1D elements along the beam axis and a distribution of quadratic LE over the cross-section domain which in all cases consists of 10 LE in the x-axis with a graded distribution towards both the free edges. A convergence study regarding the number of mathematical layers in the direction of the stacking sequence is perform, accounting from one LE per layer up to eight LE per layer. The total number of degrees of freedom goes from 10,431 for the coarsest model, to 77,805 for the finest.

In the following, the transverse stress solutions are computed for the different loading cases in $[0,90]_s$ and $[45,-45]_s$ laminates. Since this particular problem is widely used as a benchmark, only some of the most representative references are included for comparison purposes, although many others are mentioned in Section 1). The reference solutions are extracted from the original works and converted to the SI.

4.1.1 Extension

For the first assessment, the laminated beam is subjected to unitary axial strain, $\varepsilon_0 = 1$. In the proposed model, the uniform extension is modelled by prescribing the displacement u_0 in the longitudinal direction at the end section, $y = L$, as shown in Fig. 4. All the stress solutions reported in the following are obtained at half-length of the beam, $y = L/2$. The reference solutions used for this example correpond to Pipes and Pagano [45], Becker [10], Flanagan [15], Cho and Kim [17], D'Ottavio et al. [28], Dhanesh et al. [18] and Peng et al. [30]. Regarding the $[0,90]_s$ laminate, Fig. 5 shows the transverse normal stresses, σ_{zz}, across the thickness at the free-edge for an increasing number of mathematical layers per ply, from one (CUF - 1LE) to eight (CUF - 8LE). Fig. 6 includes the interlaminar stresses σ_{zz} and σ_{xz} along the interface between the 0 and 90 layers, from the center of the beam towards the free-edge. For the $[45,\text{-}45]_s$ laminate, Fig. 7 includes the transverse shear stresses across the thickness, and Fig. 8 shows the interlaminar stresses, σ_{yz} and σ_{zz} respectively, at the interface between the 45 and -45 layers.

The convergence study illustrated Figs. 5 and 7 proves that highly refined kinematics are required to compute accurate free-edge stresses by means of layerwise theories of structure. Since the only unknowns are displacements and no recovery of the 3D stress fields is performed, the trasnverse stress solutions show some discontinuities between the expansion domains (corresponding to the vertical lines in the graphs), which are more pronounced in the vicinities of the interfaces between layers due to the high stress gradients. By increasing the number of mathematical layers in the beam model, the stress distributions tend to those obtained from the exact theories, approximating well both the stress-free boundary conditions and the interlaminar continuity. It is worthy noting that in the present work an h-refinement scheme is chosen to refine the kinematics of the beam model by increasing the number of mathematical layers in the stacking direction. D'Ottavio et al. [28] also demonstrated that the transverse stress solutions are improved by adding numerical layers in the kinematic expansion of higher-order mixed plate elements. A p-refinement scheme based on hierarchical higher-order polynomials would also be suitable option, as shown in [46].

In view of these results, all the subsequent solutions of the Pipes and Pagano's laminate are obtained using eight mathematical layers per ply for all loading cases. For this model, the global distributions of all transverse stress components show an excellent agreement with the reference solutions, with some differences at the maximum value at the interlaminar singularities. This diversity cannot be considered a limitation of any theory when dealing with free-edge effects and is in all cases related to the refinement of the model, meaning that a steady increase of the peak values is expected for finner models. One can notice that the best correlation is found with the five-term solutions from Dhanesh et al. [18], which can be considered an interesting benchmark since it satisfies exactly all boundary conditions and the interlaminar continuity of displacements and stresses.

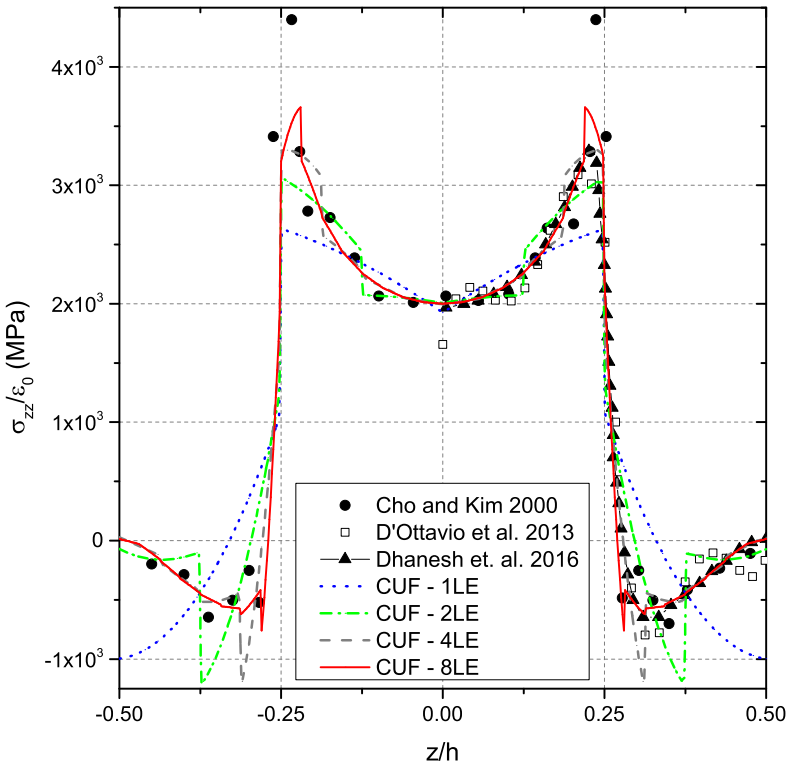

Figure 5: Transverse stresses along z of the $[0,90]_s$ laminate under extension at $x = b/2$.

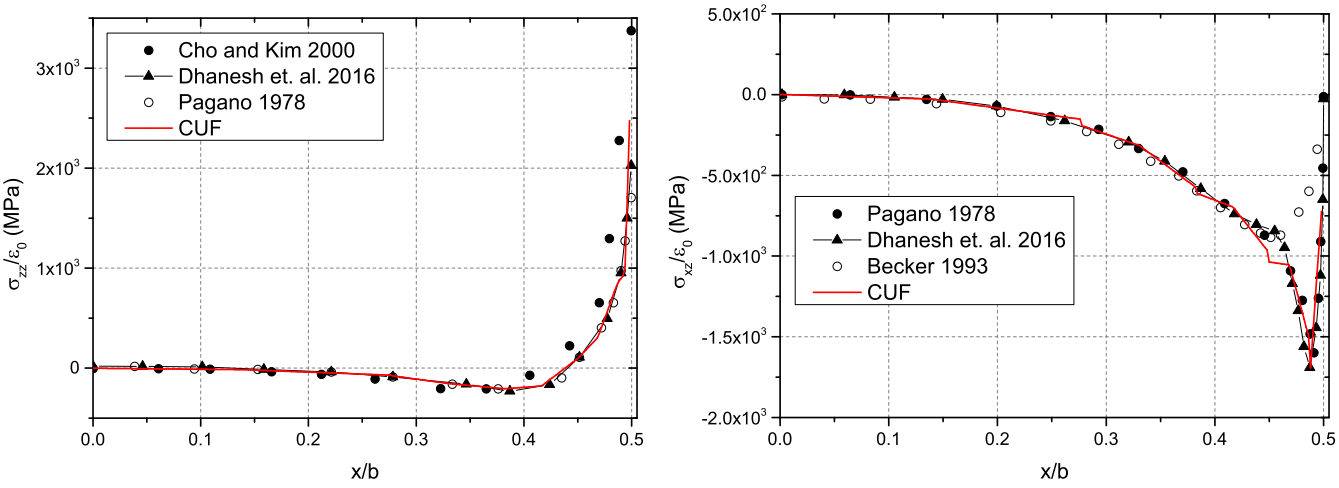

(a) σ_{zz} (b) σ_{xz}

Figure 6: Transverse stresses along x of the $[0,90]_s$ laminate under extension at $z = h/4$.

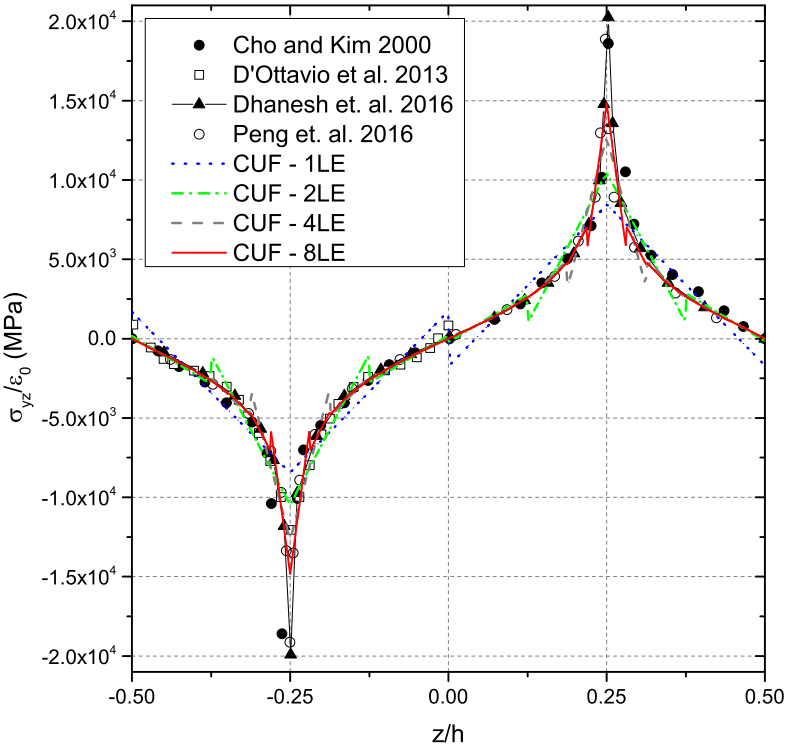

Figure 7: Transverse shear stresses along z of the $[45,\text{-}45]_s$ laminate under extension at $x = b/2$.

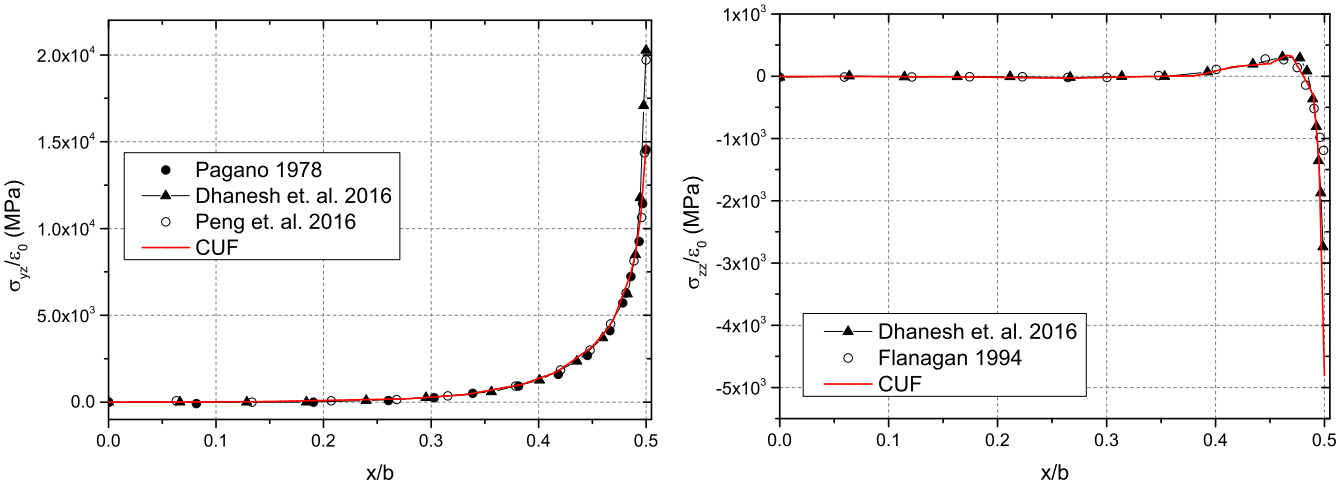

(a) σ_{yz} (b) σ_{zz}

Figure 8: Transverse stresses along x of the $[45,\text{-}45]_s$ laminate under extension at $z = h/4$.

4.1.2 Bending

Figures 9 and 10 depicts the distributions of σ_{zz} across the thickness and along the interface, respectively, of the $[0,90]_s$ laminate under uniform bending $\chi_0 = 1/t$. The reference solutions in this section are those of Cho and Kim [17] and Dhanesh et al. [18], which consider a generalized plane strain state. In order to simulate the uniform bending state in a 1D FEM model, a rotation around the x-axis of magnitude $\psi = \chi_0 \; L$ is applied at the end section, as shown in Fig. 4. The interlaminar stresses σ_{yz} and σ_{zz} of the $[45,\text{-}45]_s$ laminate are shown in Fig. 11 (a) and (b), respectively. It is possible to state that there is a good agreement with the reference solutions. In the $[45,\text{-}45]_s$ case, a better agreement is found with Cho and Kim [17], showing a faster decrease of the transverse shear stress values from the free-edge inwards in comparison to the solutions from [18].

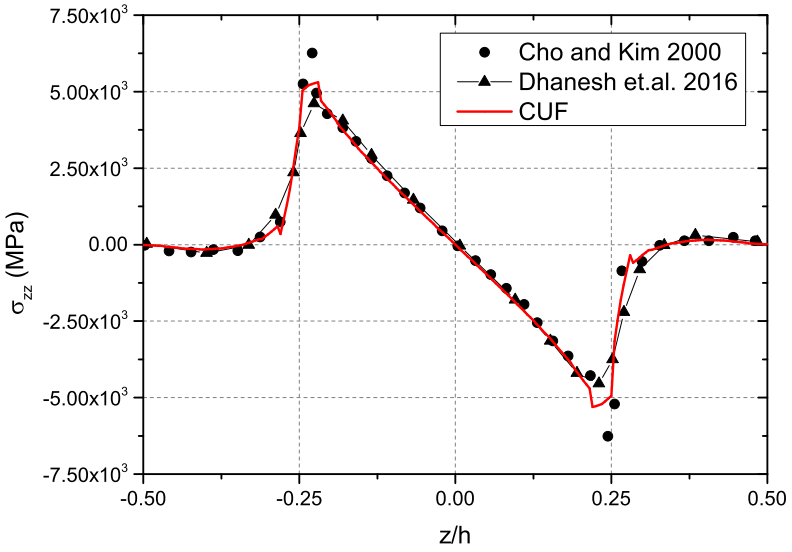

Figure 9: Transverse stresses along z of the $[0,90]_s$ laminate under bending at $x = b/2$.

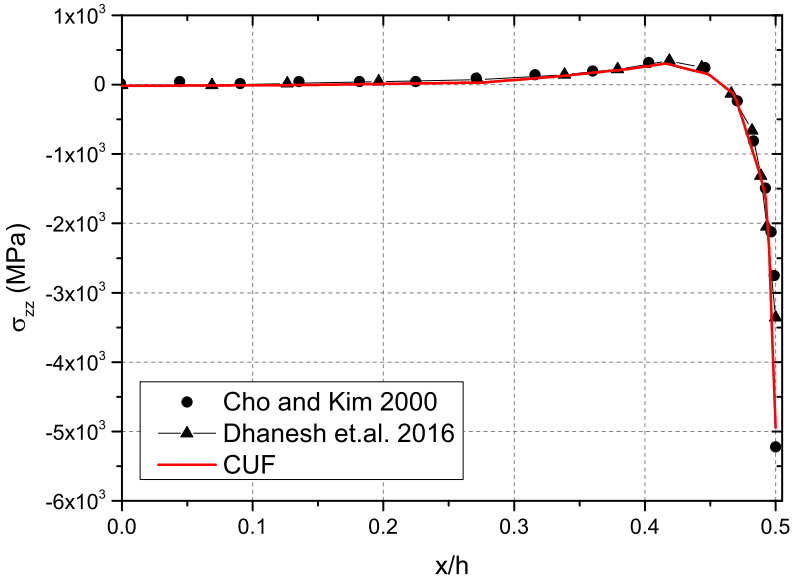

Figure 10: Transverse stresses along x of the $[0,90]_s$ laminate under bending at $z = h/4$.

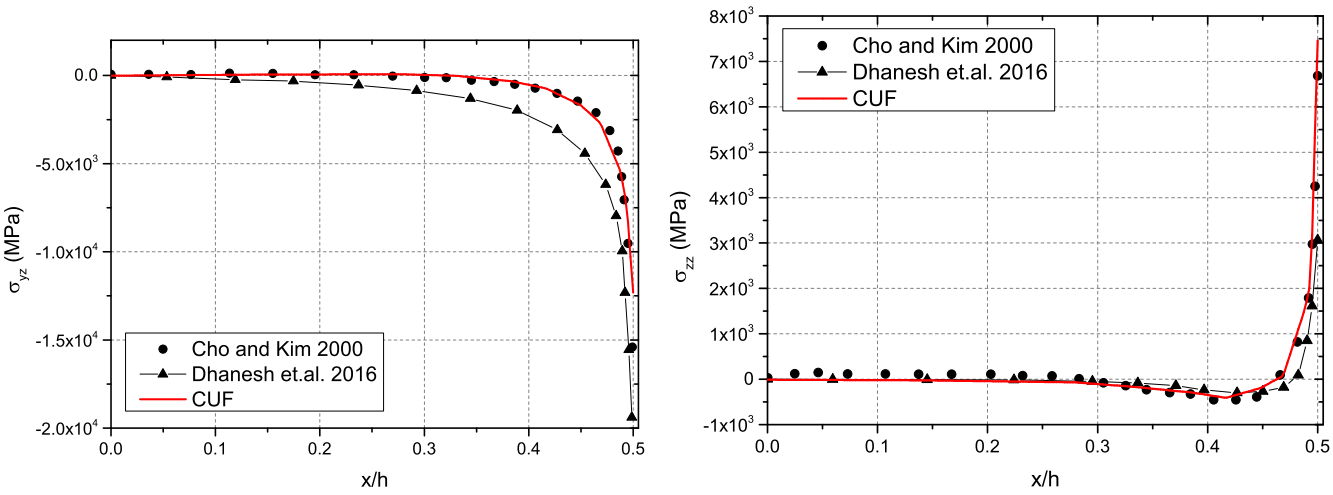

(a) σ_{yz} (b) σ_{zz}

Figure 11: Transverse stresses along x of the $[45,\text{-}45]_s$ laminate under bending at $z = h/4$.

4.1.3 Twisting

For the last benchmark assessment, the laminate is subjected to a uniform twisting $\Theta_0 = 1/t$. As for the previous example, in the present model it can be modeled by means of a rotation $\theta = \Theta_0\, L$ around the y-axis applied at the end section, as shown in Fig. 4. The reference solutions are extracted from Cho and Kim [17], Dhanesh et al. [18] and Yin [12]. The stress distributions that arise at the free edges under twisting differ from those of the previous cases in that no singularity is observed at the vicinities of the interfaces and the maximum value of the transverse stresses is located at the center of the thickness. Figure 12 shows the normal stresses σ_{zz} along the interface between the 0 and 90 layers, whereas Figs. 13 and 14 includes the transverse shear stresses σ_{yz} along the interface between distinct plies and across the thickness, respectively. Again, all the solutions presented in the graphs follow the same trend, with some differences at the maximum values at $x = b/2$. The best agreement is found with [18], as it can be observed in Fig. 14.

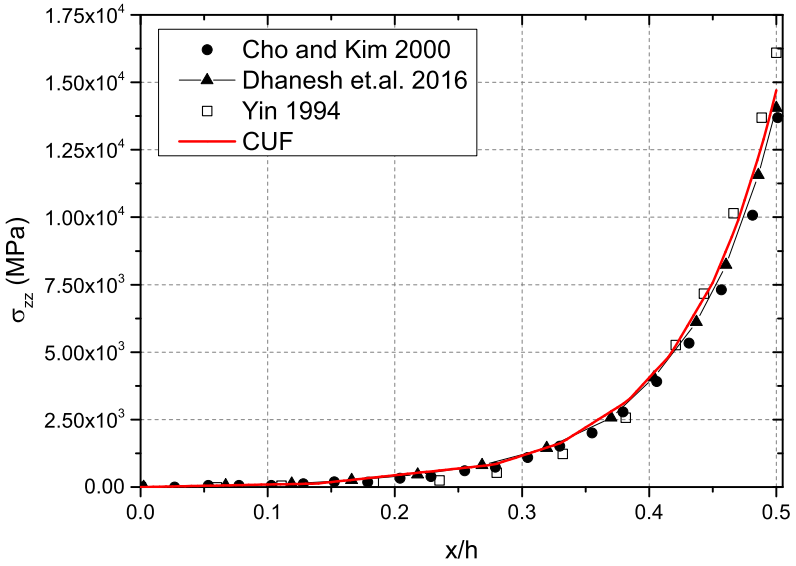

Figure 12: Transverse stresses along x of the $[0,90]_s$ laminate under twisting at $z = h/4$.

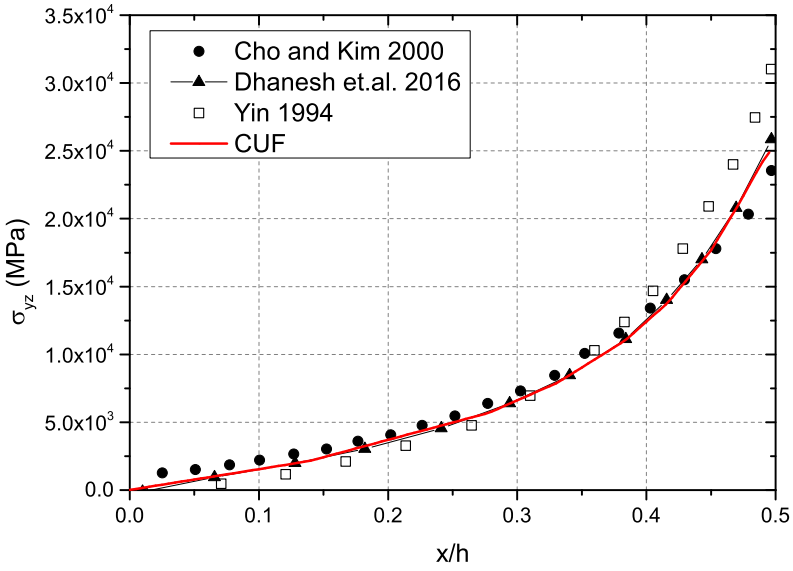

Figure 13: Transverse shear stresses along x of the $[45,\text{-}45]_s$ laminate under bending twisting at $z = h/4$.

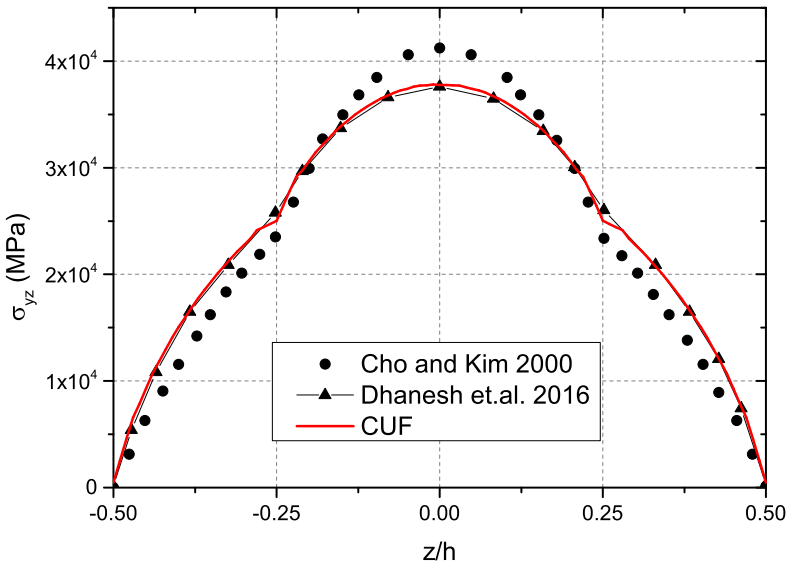

Figure 14: Transverse shear stresses along z of the $[45,\text{-}45]_s$ laminate under twisting at $x = b/2$.

4.2 Free-edge effects in complex parts

After validating the fidelity of the stress solutions against the literature, the capabilities of the model for the efficient free-edge analysis in complex composite structures and generic three-dimensional boundary conditions is presented in this section. A C-section composite beam, typically used as reinforcement of lightweight structures, is herein modeled and three different load cases are considered. The geometry of the problem is depicted in Fig. 15. The composite lay-up consists of a four-ply [0,90,45,-45] of IM7/8552 material, with the following ply mechanical properties:

$$\begin{aligned} &E_1 = 165\ GPa, \quad E_2 = 9\ GPa, \quad E_3 = 9\ GPa, \\ &G_{12} = 5.6\ GPa, \quad G_{13} = 5.6\ GPa, \quad G_{23} = 2.8\ GPa, \\ &\nu_{12} = 0.34, \quad \nu_{13} = 0.34, \quad \nu_{23} = 0.5. \end{aligned} \tag{12}$$

All the plies are of equal thickness, $t = 0.635$ mm, and they are stack from inside towards the exterior, see Fig. 15. The loading cases considered, which are shown in Fig. 16, are described as follows:

- Load case 1: the beam is clamped at one end, $y = 0$, and prescribed displacements $\bar{\boldsymbol{u}}(x, L, z) = [0, 0.02, 0]$ m are applied in the other end section.
- Load case 2: the beam is supported at both ends and a distributed vertical load of $p_z = -1$ kPa is applied over the top surface.
- Load case 3: the beam is clamped at one end, $y = 0$, and a distributed shear load $p_x = -1$ kPa is applied over the top surface.

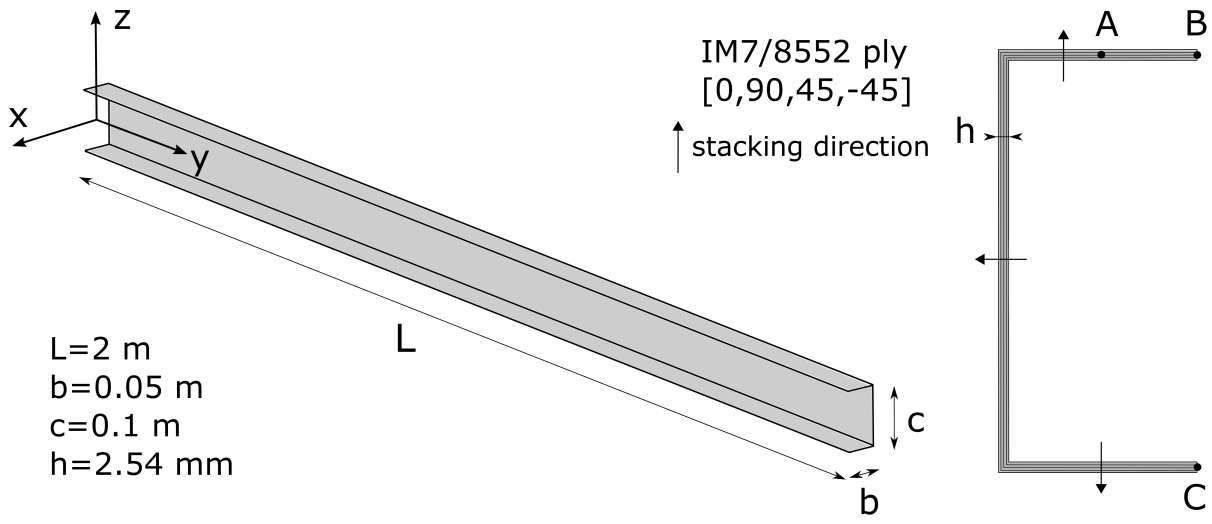

Figure 15: Geometry and dimensions of the composite C-beam.

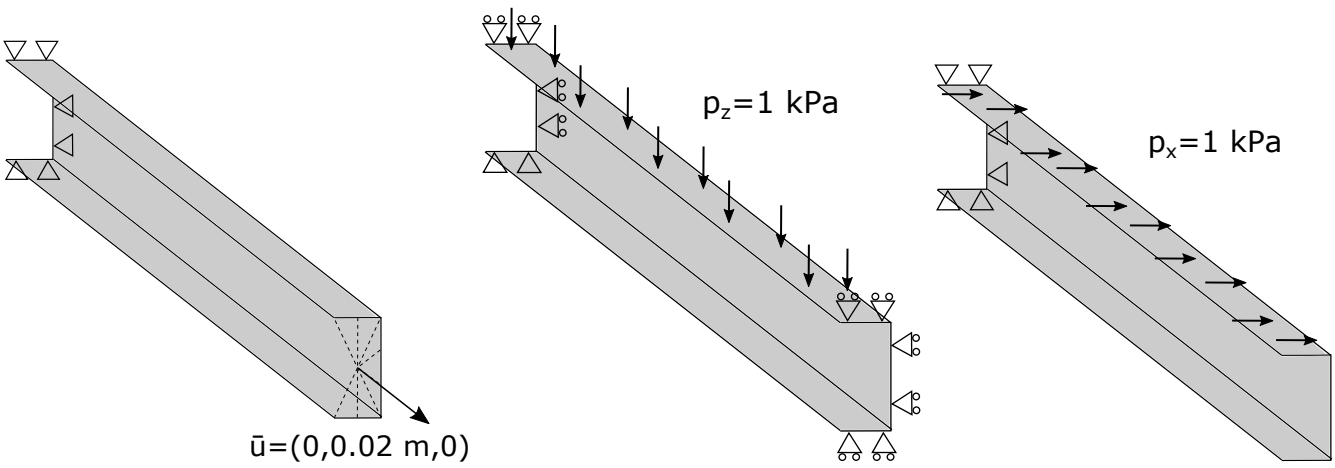

(a) Load case 1 (b) Load case 2 (c) Load case 3

Figure 16: Representation of the three load cases analyzed.

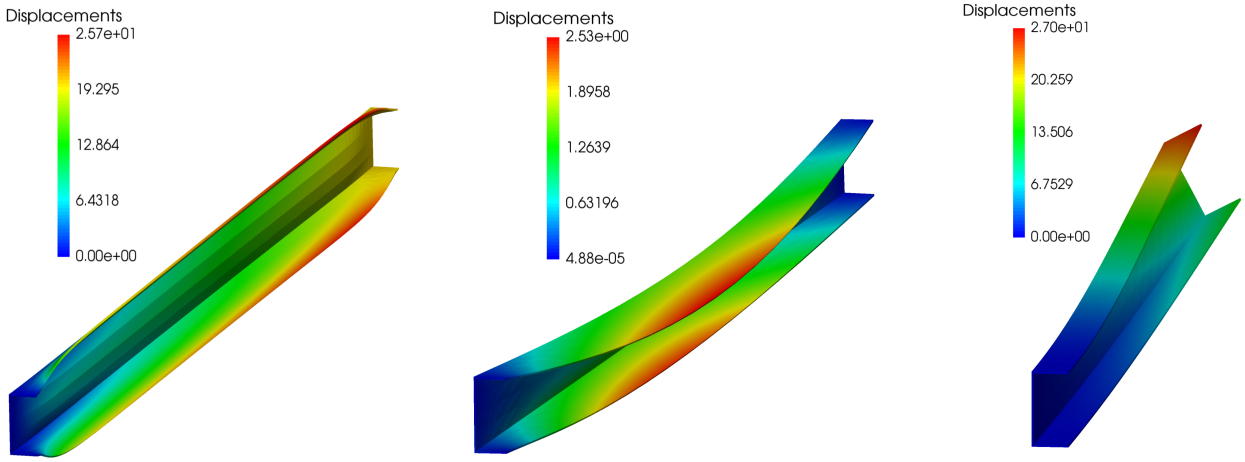

(a) Load case 1 (b) Load case 2 (c) Load case 3

Figure 17: Deformation and contour of the total displacements.

Figure 17 shows the deformations of the composite beam for all load cases considered. It is possible to observe that in all three cases non-classical effects arise, including warping, in-plane deformation of the cross-section and secondary bending, which may have an effect on the stress fields at the free-edges. For the sake of comparison and assessment, different 2D and 3D FEM models are generated in the commercial software MSC Nastran [47]. A brief description of these is included in Table 1, which gives information about the computational models and the maximum total displacements obtained for each case. All models are within 4 % of error in displacements. The Nastran 2D model is used only for load case 1 with the purpose of comparing the in-plane stresses obtained from the CUF model in complex structures. For that, the stress fields across the thickness at the center of the top flange (point A in Fig. 15) are plotted in Fig. 18. From both models it is possible to observe the presence of secondary bending due to the rise of σ_{xx} in the 90° layer. It is also worthy noting that classical plate theories cannot capture the linear distribution of in-plane stresses under bending, which might affect the evaluation failure indexes.

Table 1: Model description and displacement solutions.

Model	Description	DOF	Maximum displacement [mm]		
			Load case 1	Load case 2	Load case 3
CUF	8 4-node 1D elements + 280 L9, 5 domains per layer (similar to Fig. 2)	89,175	25.79	2.53	27.01
Nastran 2D	7800 QUAD4 elements	40,200	26.87	-	-
Nastran 3D - 1	108,000 linear HEX8 elements, 1 element per layer	410,865	26.36	2.61	26.55
Nastran 3D - 3	1,800,000 linear HEX8 elements, 3 element per layer	2,276,739	26.50	2.63	26.69

*All models are refined towards the free-edges

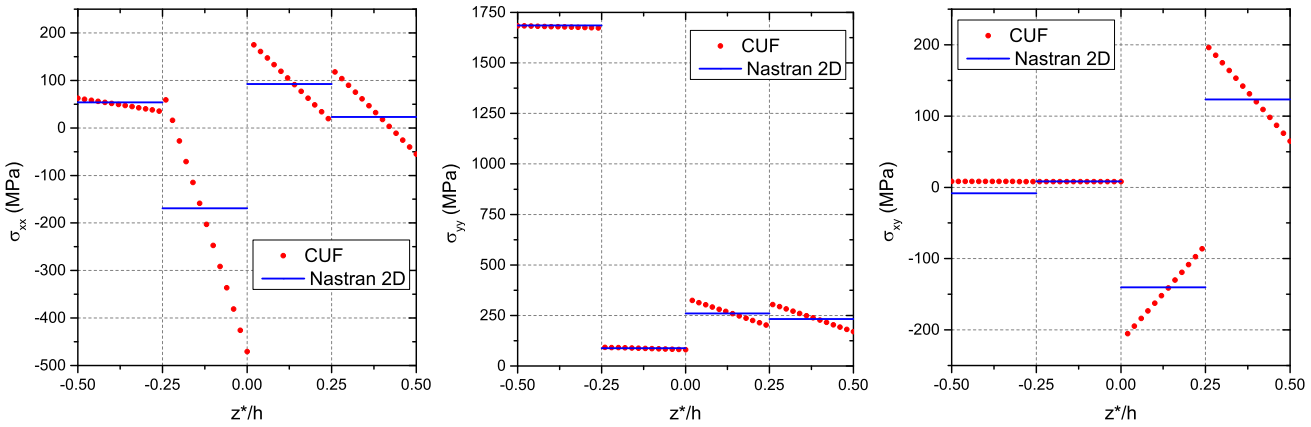

(a) σ_{xx} (b) σ_{yy} (c) σ_{xy}

Figure 18: In-plane stresses of the composite C-beam at Point A of the midspan section.

The free-edge stress distributions are evaluated in the center of the structure at the top flange for all three load cases. The results obtained from the proposed model and the Nastran 3D models are included in Figs. 19, 21 and 22. As expected, some similarities are found with the benchmark results included in the previous section. In the first two cases, the maximum shear stress σ_{yz} is located at the interface between the 45° and −45° layers, whereas the maximum normal stress σ_{zz} corresponds to the 90° layer, close to the 45° interface. However, in load case 3 the situation is the opposite. Figure 20 shows the most relevant interlaminar stresses in the vicinity of the free-edge. It is possible to note that the free-edge effects are also in this case confined in a small region of depth about one thickness of the laminate, h.

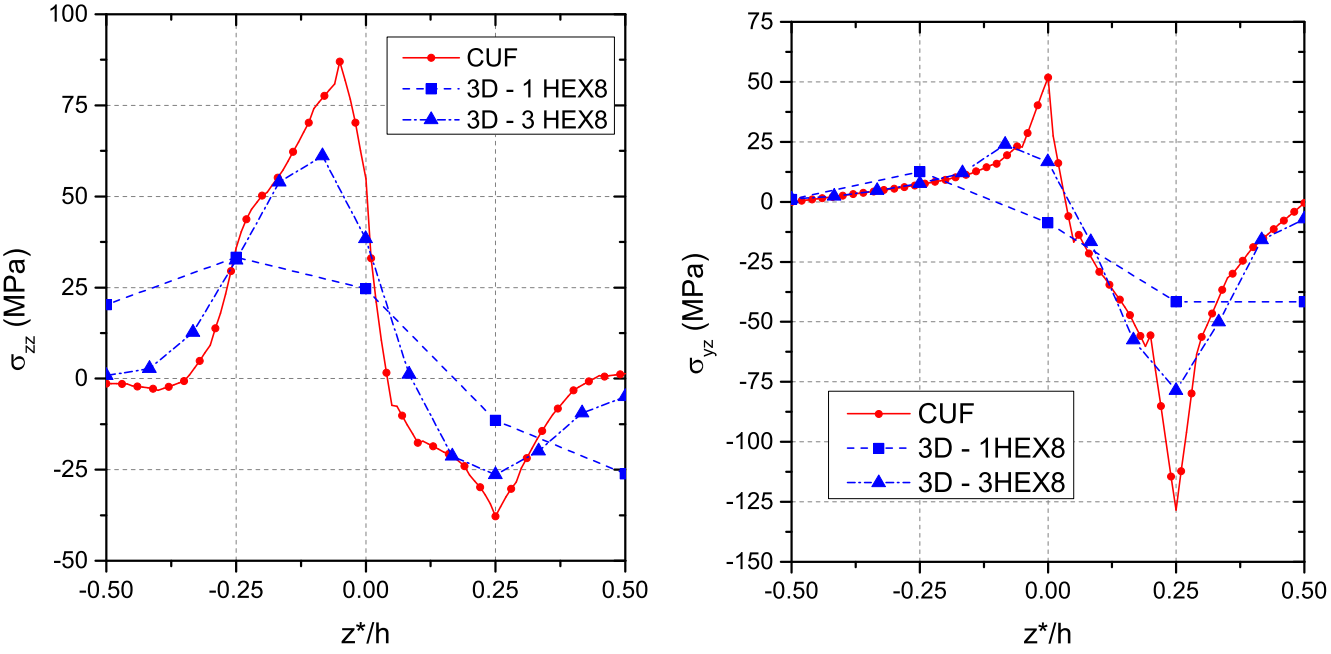

(a) Normal stress

(b) Shear stress

Figure 19: Free edge stresses of the composite C-beam at midspan, point B, for load case 1.

Finally, a further study was performed on the relation between the local deformation state of the structure and the severity of the stress concentrations in the free edges. Figures 23 and 24 show the stress concentrations at different points along the beam structure for load cases 2 and 3. In general 3D problems, the variation of the local deformation state over the structure lead to different profiles of the transverse stresses along the free edges, which should be understood for the correct failure evaluation of the composite. Indeed, although there is a clear relation between the local extension and the free-edge effects, see Fig. 24, the maximum value of the stress peaks does not necessarily correspond to the location of the maximum local deformation of the flange (point F), as shown in Fig. 23. This kind of results cannot be obtained using semi-analytical models based on generalized plane strains and represent the main novelty of the present work.

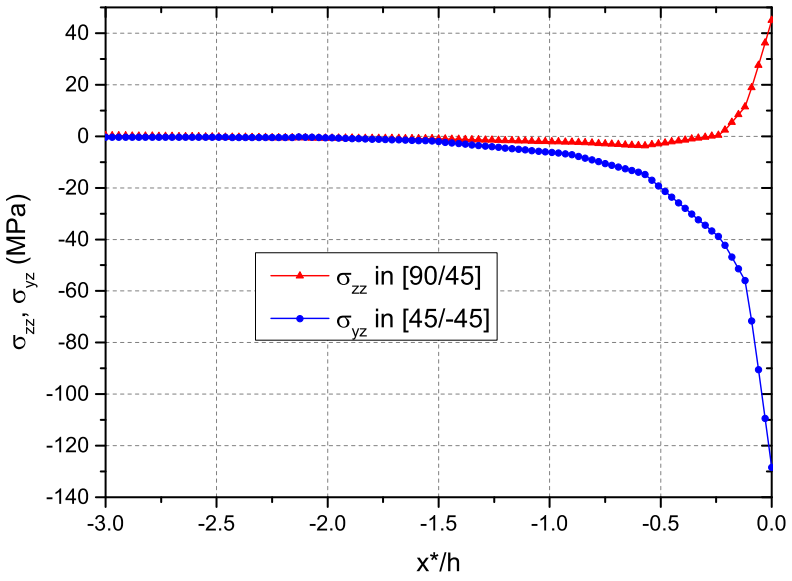

Figure 20: Interlaminar stresses of the composite C-beam at the top-flange. The $x*$-axis starts at the free-edge and the negative values refer to the depth inside the laminate.

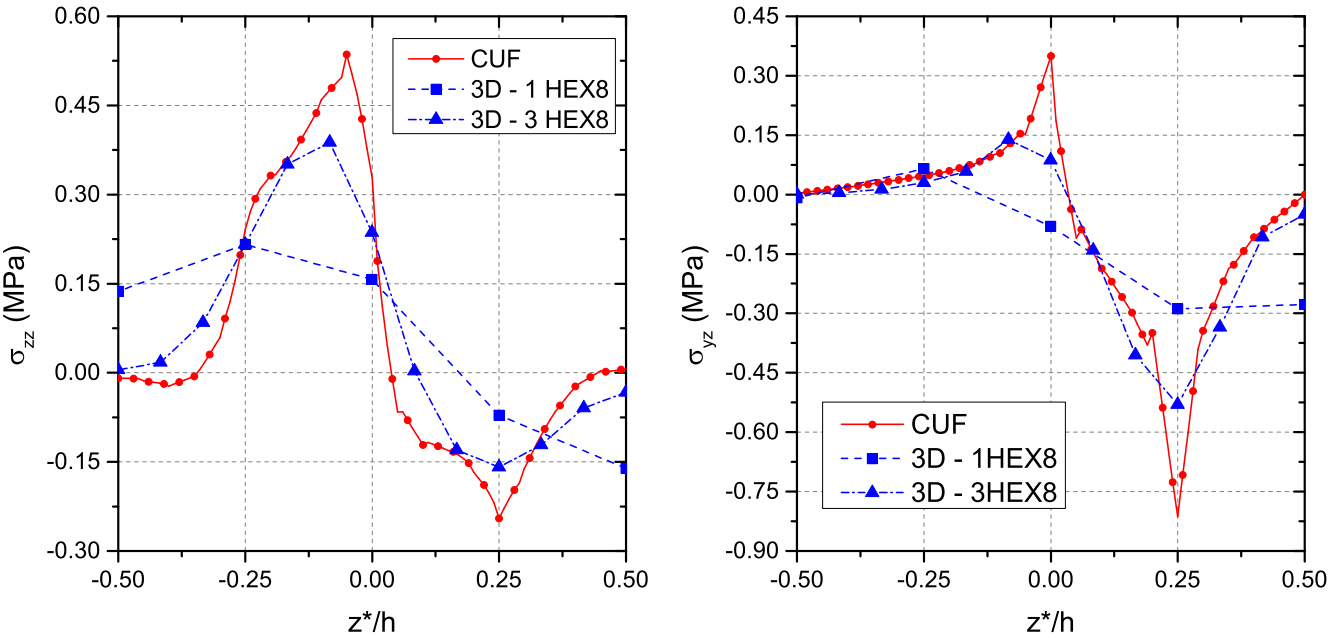

(a) Normal stress

(b) Shear stress

Figure 21: Free edge stresses of the composite C-beam at midspan, point B, for load case 2.

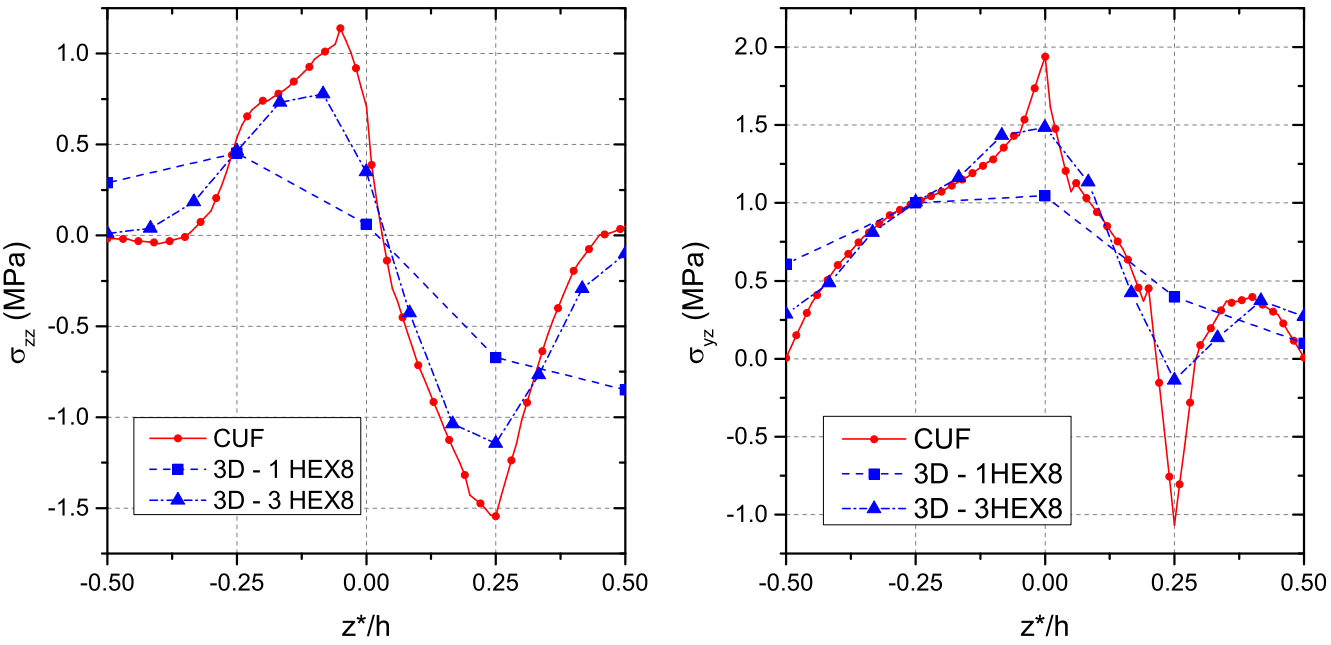

(a) Normal stress (b) Shear stress

Figure 22: Free edge stresses of the composite C-beam at midspan, point B, for load case 3.

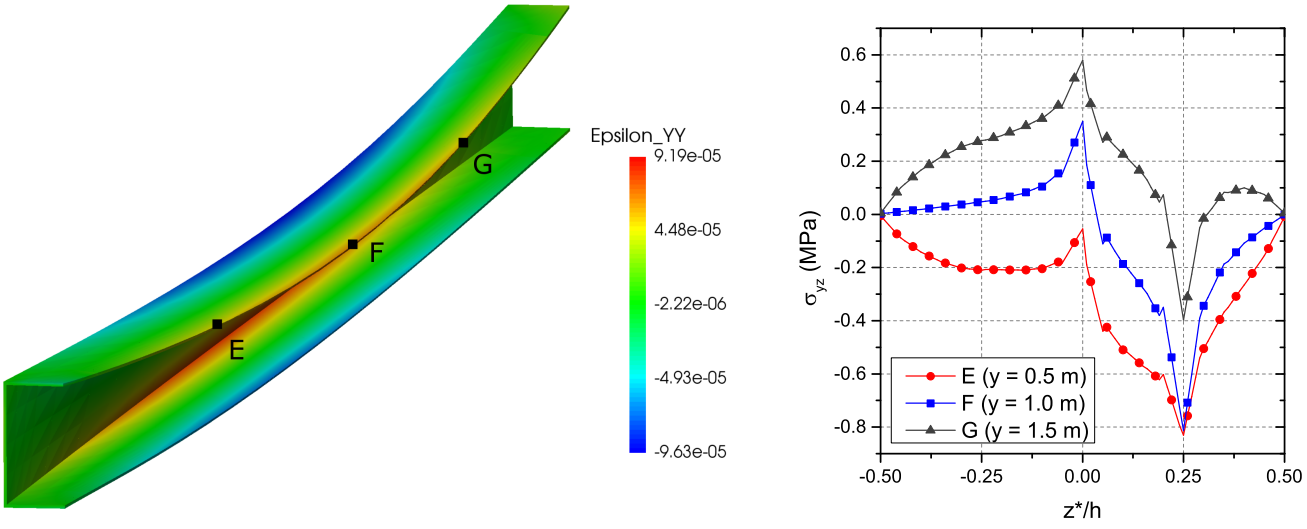

(a) Longitudinal strain contour (b) Shear stress

Figure 23: Effect of local deformation on the free-edge stress fields, load case 2.

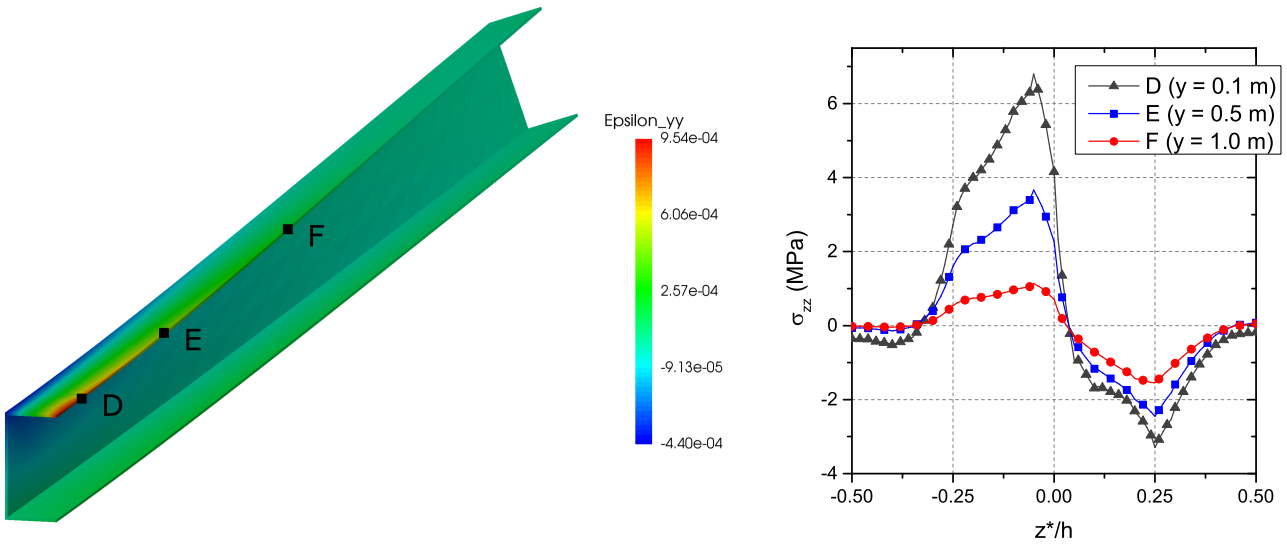

(a) Longitudinal strain contour

(b) Normal stress

Figure 24: Effect of local deformation on the free-edge stress fields, load case 3.

5 Conclusion

The present work introduces an efficient modeling technique for the free-edge analysis of generic composite parts. The model is developed in the framework of the Carrera's unified formulation and is based on the use of advanced 1D elements with LW kinematics. The displacement field is enriched with only displacement unknowns that are interpolated over the cross-section domain by means of Lagrange functions, allowing the model to capture the complex stress fields that arise at the free-edges of laminated structures. First, a comprehensive assessment of the Pipes and Pagano problem [4] is carried out, showing the accuracy and robustness of the model under extension, bending and twisting loads. Subsequently, the capabilities of the model are fully exploited to present new results of free-edge effects in a composite C-beam stringer.

In view of the results, the authors believe that the proposed methodology can be used to fill the gap between the available theories for free-edge analysis, which provide highly accurate results for a small range of geometries and loading conditions, and the FE analysis of complex composite structures, which cannot be employed to study these singularities due to computational limits. Further developments will be focused on the free-edge analysis of curved laminates and the use of the model as a global-local tool for real-life structures. The introduction of a stress-displacement formulation based on the Reissner's mixed variational theorem is also of interest in the current framework.

A Geometrical and constitutive relations

The second-order strain and stress tensors, expressed in vectorial form, can be written as:

$$\begin{aligned} \boldsymbol{\varepsilon}^T &= \left\{ \begin{array}{cccccc} \varepsilon_{yy} & \varepsilon_{xx} & \varepsilon_{zz} & \varepsilon_{xz} & \varepsilon_{yz} & \varepsilon_{xy} \end{array} \right\} \\ \boldsymbol{\sigma}^T &= \left\{ \begin{array}{cccccc} \sigma_{yy} & \sigma_{xx} & \sigma_{zz} & \sigma_{xz} & \sigma_{yz} & \sigma_{xy} \end{array} \right\} \end{aligned} \tag{13}$$

with no loss of generality. The coordinate system defined by x, y and z corresponds to that of Fig. 1. The Green-Cauchy strain-displacement relations are considered as geometrical relations:

$$\boldsymbol{\varepsilon} = \mathbf{D}\,\mathbf{u} \tag{14}$$

$\mathbf{D}$ being the following linear differential operator:

$$\mathbf{D} = \begin{bmatrix} 0 & \frac{\partial}{\partial y} & 0 \\ \frac{\partial}{\partial x} & 0 & 0 \\ 0 & 0 & \frac{\partial}{\partial z} \\ \frac{\partial}{\partial z} & 0 & \frac{\partial}{\partial x} \\ 0 & \frac{\partial}{\partial z} & \frac{\partial}{\partial y} \\ \frac{\partial}{\partial y} & \frac{\partial}{\partial x} & 0 \end{bmatrix} \tag{15}$$

On the other hand, the Hooke's law is applied at the ply level to obtain the stresses:

$$\boldsymbol{\sigma} = \mathbf{C}\,\boldsymbol{\varepsilon} \tag{16}$$

where $\boldsymbol{C}$ is the stiffness matrix of the material (orthotropic), defined as:

$$\mathbf{C} = \begin{bmatrix} C_{33} & C_{23} & C_{13} & 0 & 0 & 0 \\ C_{23} & C_{22} & C_{12} & 0 & 0 & 0 \\ C_{13} & C_{12} & C_{11} & 0 & 0 & 0 \\ 0 & 0 & 0 & C_{44} & 0 & 0 \\ 0 & 0 & 0 & 0 & C_{55} & 0 \\ 0 & 0 & 0 & 0 & 0 & C_{66} \end{bmatrix} \tag{17}$$

3 refers to the fiber direction and 1 lies perpendicular to the lamina. For generic orientations of the laminate in the global coordinate system, the stiffness matrix is rotated according to Fig. 25, and the Hooke's law is rewritten as:

$$\boldsymbol{\sigma} = \tilde{\mathbf{C}}^k\,\boldsymbol{\varepsilon} \tag{18}$$

The components of the rotated stiffness matrix, $\tilde{\mathbf{C}}^k$, depend now on the angles θ and ψ.

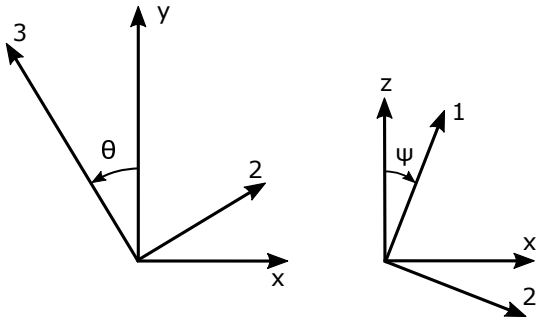

Figure 25: Rotations of the lamina.

References

[1] R. M. Jones. *Mechanics of composite materials*. Taylor and Francis Ltd., London, UK, 2^{nd} edition, 1998.

[2] T. Hayashi. Analytical study of interlaminar shear stresses in a laminated composite plate. *Transaction of Japan Society for Aeronautical Engineering and Space Science*, 66:43–48, 1967.

[3] A.H. Puppo and H.A. Evensen. Interlaminar shear in laminated composites under generalized plane stress. *Journal of Composite Materials*, 4(2):204–220, 1970.

[4] R.B. Pipes and N.J. Pagano. Interlaminar stresses in composite laminates under uniform axial extension. *Journal of Composite Materials*, 4(4):538–548, 1970.

[5] C. Mittelstedt and W. Becker. Interlaminar stress concentrations in layered structures: Part i - a selective literature survey on the free-edge effect since 1967. *Journal of Composite Materials*, 38(12):1037–1062, 2004.

[6] R.B. Pipes and N.J. Pagano. Interlaminar stresses in composite laminates - an approximate elasticity solution. *Journal of Applied Mechanics*, 41(3):668–672, 1974.

[7] N.J. Pagano. On the calculation of interlaminar normal stress in composite laminate. *Journal of Composite Materials*, 8:65–81, 1974.

[8] J.M. Whitney and C.T. Sun. A higher order theory for extensional motion of laminated composites. *Journal of Sound and Vibration*, 30(1):85 – 97, 1973.

[9] C. Kassapoglou and P. A. Lagace. Closed form solutions for the interlaminar stress field in angle-ply and cross-ply laminates. *Journal of Composite Materials*, 21(4):292–308, 1987.

[10] W. Becker. Closed-form solution for the free-edge effect in cross-ply laminates. *Composite Structures*, 26(1):39 – 45, 1993.

[11] S.G. Lekhniskii. *Anisotropic plates*. Gordon & Breach, New York, 1968. translated from 2nd russian Edition by S.W. Tsai and T. Cheron.

[12] W.L. Yin. Free-edge effects in anisotropic laminates under extension, bending, and twisting, part ii: Eigenfunction analysis and the results for symmetric laminates. *Journal of Applied Mechanics*, 61(2):416–421, 1994.

[13] M. Tahani and A. Nosier. Edge effects of uniformly loaded cross-ply composite laminates. *Materials and Design*, 24(8):647 – 658, 2003.

[14] J. N. Reddy. A generalization of two dimensional theories of laminated composite plates. *Communications in Applied Numerical Methods*, 3(3):173–180.

[15] G. Flanagan. An efficient stress function approximation for the free-edge stresses in laminates. *International Journal of Solids and Structures*, 31(7):941 – 952, 1994.

[16] M. Cho and J. Y. Yoon. Free-edge interlaminar stress analysis of composite laminates by extended kantorovich method. *AIAA Journal*, 37(5):656–660, 1999.

[17] M. Cho and H. S. Kim. Iterative free-edge stress analysis of composite laminates under extension, bending, twisting and thermal loadings. *International Journal of Solids and Structures*, 37(3):435 – 459, 2000.

[18] N. Dhanesh, S. Kapuria, and G. G. S. Achary. Accurate prediction of three-dimensional free edge stress field in composite laminates using mixed-field multiterm extended kantorovich method. *Acta Mechanica*, 228(8):2895–2919, Aug 2017.

[19] E. Reissner. On a certain mixed variational theorem and a proposed application. *International Journal for Numerical Methods in Engineering*, 20(7):1366–1368, 1984.

[20] A.S.D. Wang and Frank W. Crossman. Some new results on edge effect in symmetric composite laminates. *Journal of Composite Materials*, 11(1):92–106, 1977.

[21] J.D. Whitcomb, I.S. Raju, and J.G. Goree. Reliability of the finite element method for calculating free edge stresses in composite laminates. *Computers and Structures*, 15(1):23 – 37, 1982.

[22] I.S. Raju and J. H. Crews. Interlaminar stress singularities at a straight free edge in composite laminates. *Computers and Structures*, 14(1):21 – 28, 1981.

[23] Larry B. Lessard, Andrew S. Schmidt, and Mahmood M. Shokrieh. Three-dimensional stress analysis of free-edge effects in a simple composite cross-ply laminate. *International Journal of Solids and Structures*, 33(15):2243 – 2259, 1996.

[24] E. Martin, D. Leguillon, and N. Carrère. A twofold strength and toughness criterion for the onset of free-edge shear delamination in angle-ply laminates. *International Journal of Solids and Structures*, 47(9):1297 – 1305, 2010.

[25] G. Davì and A. Milazzo. Boundary element solution for free edge stresses in composite laminatess. *Journal of Applied Mechanics*, 64(4):877 – 884, 1997.

[26] J. Lindemann and W. Becker. Analysis of the free-edge effect in composite laminates by the boundary finite element method. *Mechanics of Composite Materials*, 36(3):207–214, May 2000.

[27] D. H. Robbins and J. N. Reddy. Modelling of thick composites using a layerwise laminate theory. *International Journal for Numerical Methods in Engineering*, 36(4):655–677, 1993.

[28] M. D'Ottavio, P. Vidal, E. Valot, and O. Polit. Assessment of plate theories for free-edge effects. *Composites Part B: Engineering*, 48:111 – 121, 2013.

[29] P. Vidal, L. Gallimard, and O. Polit. Assessment of variable separation for finite element modeling of free edge effect for composite plates. *Composite Structures*, 123:19 – 29, 2015.

[30] B. Peng, J. Goodsell, R.B. Pipes, and W. Yu. Generalized free-edge stress analysis using mechanics of structure genome. *Journal of Applied Mechanics*, 83(10):101013–7, 2016.

[31] E. Carrera, M. Cinefra, E. Zappino, and M. Petrolo. *Finite Element Analysis of Structures Through Unified Formulation*. John Wiley and Sons, Ltd, 2014.

[32] E. Carrera and M. Petrolo. Refined beam elements with only displacement variables and plate/shell capabilities. *Meccanica*, 47(3):537–556, 2012.

[33] E. Carrera and M. Petrolo. Refined one-dimensional formulations for laminated structure analysis. *AIAA Journal*, 50(1):176–189, 2012.

[34] E. Carrera, M. Maiarú, and M. Petrolo. Component-wise analysis of laminated anisotropic composites. *International Journal of Solids and Structures*, 49(13):1839 – 1851, 2012.

[35] E. Carrera, M. Filippi, P.K. Mahato, and A. Pagani. Accurate static response of single- and multi-cell laminated box beams. *Composite Structures*, 136:372 – 383, 2016.

[36] S. Srinivas. A refined analysis of composite laminates. *Journal of Sound and Vibration*, 30(4):495 – 507, 1973.

[37] E.I. Grigoliuk and G.M. Kulikov. "general direction of development of the theory of multilayer shells. *Mekhanika Kompozitnykh Materialov*, 24(2):287 – 298, 1988. In Russian; translation in Mech. Compos. Materials 24:2 (1988), 231–241.

[38] K. Surana and S. Nguyen. Two-dimensional curved beam element with higher-order hierarchical transverse approximation for laminated composites. *Computers and Structures*, 36:499–511, 1990.

[39] R. P. Shimpi and Y. M. Ghugal. A new layerwise trigonometric shear deformation theory for two-layered cross-ply beams. *Composites Science and Technology*, 61(9):1271 – 1283, 2001.

[40] M. Tahani. Analysis of laminated composite beams using layerwise displacement theories. *Composite Structures*, 79(4):535 – 547, 2007.

[41] J. N. Reddy. *Mechanics of laminated composite plates and shells. Theory and Analysis*. CRC Press, 2^{nd} edition, 2004.

[42] E. Carrera. C0 Reissner-Mindlin multilayered plate elements including zig-zag and interlaminar stress continuity. *International Journal for Numerical Methods in Engineering*, 39(11):1797–1820, 1996.

[43] R. B. Pipes. Moiré analysis of the interlaminar shear edge effect in laminated composites. *Journal of Composite Materials*, 5(2):255–259, 1971.

[44] N. Saeedi, K. Sab, and Je.-F. Caron. Delaminated multilayered plates under uniaxial extension. part i: Analytical analysis using a layerwise stress approach. *International Journal of Solids and Structures*, 49(26):3711 – 3726, 2012.

[45] N.J. Pagano. Stress fields in composite laminates. *International Journal of Solids and Structures*, 14(5):385 – 400, 1978.

[46] E. Carrera, A.G. de Miguel, and A. Pagani. Hierarchical theories of structures based on legendre polynomial expansions with finite element applications. *International Journal of Mechanical Sciences*, 120:286 – 300, 2017.

[47] MSC.Software Corporation. MD Nastran 2010 Quick Reference Guide. 2010.